Inorganic Chemistry

Communication

pubs.acs.org/IC

Avoiding Magnetochemical Overparametrization, Exemplified by One-Dimensional Chains of Hexanuclear Iron(III) Pivalate Clusters

Svetlana G. Baca,[†] Tim Secker,[†] Annabel Mikosch,[†] Manfred Speldrich,[†] Jan van Leusen,[†] Arkady Ellern,[‡] and Paul Kögerler*[,†]

[†]Institute of Inorganic Chemistry, RWTH Aachen University, 52074 Aachen, Germany

[‡]Ames Laboratory, Iowa State University, Ames, Iowa 50011, United States

Supporting Information

ABSTRACT: One-dimensional chain coordination polymers based on hexanuclear iron(III) pivalate building blocks and 1,4-dioxane (diox) or 4,4′-bipyridine (4,4′-bpy) bridging ligands, $[Fe_6O_2(O_2CH_2)(O_2CCMe_3)_{12}(diox)]_n$ (**1**) and $[Fe_6O_2(O_2CH_2)(O_2CCMe_3)_{12}(4,4'\text{-bpy})]_n$ (**2**), showcase the utility of the angular overlap model, implemented in the program *wxJFinder*, in the predictive identification of the relative role of intra- and intercluster coupling.

Coordination cluster polymers (CPs) built up from magnetic polynuclear coordination clusters have received considerable attention because of potential applications in several fields.[1] The rational preparation of such CPs, in particular the controlled integration of the individual cluster properties into those of the final, networked system, represents multiple challenges. Taking advantage of the iron(III) and manganese(II,III) polynuclear carboxylate clusters in the preparation of magnetic coordination polymers, we reported a large variety of cluster-based CPs where building cluster blocks range from tri- and tetranuclear carboxylate clusters (for Fe- and Mn-containing CPs) to hexanuclear carboxylate clusters (for Mn-containing CPs).[2−5] The interpretation of the magnetic characteristics of CPs based on microscopic model Hamiltonians is, however, complicated by the additional intercluster coupling. While this can be accounted for by several models, e.g., the molecular-field approach, adding even one additional independent parameter to the fitting procedure that relates the experimental magnetic data to the model Hamiltonian can result in isospectrality issues, i.e., in multiple sets of model parameters that all result in virtually identical quality-of-fit indicators. Circumventing this overparametrization problem thus mandates constraints to the fitting parameters and reasonable starting values. Yet, even if the individual cluster building blocks of CPs exist as discrete (noncoupled) species, the geometrical distortions introduced by the polymerization mean different intracluster coupling. We herein showcase how the semiempirical program *wxJFinder*, implementing the angular overlap model (AOM), provides accurate predictions for Heisenberg−Dirac−van Vleck-type exchange energies. Using our computational framework CONDON,[6] we demonstrate how this approach can be used to accurately describe both intra- and intercluster interactions in the first examples of CPs based on hexanuclear iron(III) clusters. In these two compounds, aliphatic O,O′ or aromatic N,N′ connectors link hexairon(III) pivalate clusters into one-dimensional (1D) chains, resulting in $[Fe_6O_2(O_2CH_2)(O_2CCMe_3)_{12}(diox)]_n$ (**1**) and $[Fe_6O_2(O_2CH_2)(O_2CCMe_3)_{12}(4,4'\text{-bpy})]_n$ (**2**) (diox = 1,4-dioxane; 4,4′-bpy = 4,4′-bipyridine). **1** has been prepared from smaller μ_3-oxo trinuclear $[Fe_3O(O_2CCMe_3)(H_2O)_3](O_2CCMe_3)\cdot 2Me_3CCO_2H$ or hexanuclear $[Fe_6O_2(OH)_2(O_2CCMe_3)_{12}]$ species by the slow diffusion of MeCN into its solution in diox, whereas the reaction of a hexanuclear iron(III) pivalate with 4,4′-bpy in the presence of 2,2′-bpy in a CH_2Cl_2/MeCN solution (1:1) under heating yields **2**.

Single-crystal X-ray diffraction analysis[7] of both **1** and **2** identifies the μ_3-oxo hexanuclear $[Fe_6O_2(O_2CH_2)(O_2CCMe_3)_{12}]$ building block, linked via diox (**1**) or 4,4′-bpy (**2**) into 1D zigzag chains (Figure 1), with shortest Fe···Fe distances between neighboring hexanuclear clusters of 7.171 Å (**1**) and 11.393 Å (**2**).

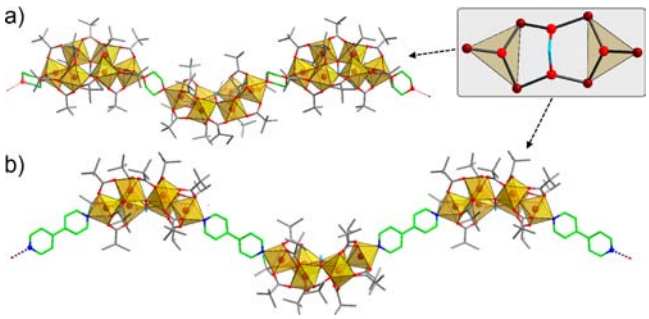

Figure 1. Structures of the 1D chains in **1** (a) and **2** (b). Iron coordination environments are shown as yellow polyhedra. Color code: C (bridging ligands), green; O, red; N, dark blue; C, gray. Inset: view of the $[Fe_6O_2(O_2CH_2)]^{12+}$ core structure in **1** and **2**. The C atom of the methanediolate group is shown in light blue. Carboxylate groups and H atoms are omitted for clarity.

In both CPs, the cores of six corner-sharing FeO_6 or FeO_5N octahedra comprise two $[Fe_3(\mu_3\text{-}O)]^{7+}$ units, with their Fe centers being bridged by five pivalate groups, and two carboxylate residues further link these μ_3-oxo trinuclear units $[Fe_3(\mu_3\text{-}O)(O_2CCMe_3)_5)]^{2+}$ into hexanuclear clusters. The main feature of the Fe_6 metallic core is the presence of a rare

Received: February 15, 2013
Published: March 27, 2013

   dx.doi.org/10.1021/ic4003884 | *Inorg. Chem.* 2013, 52, 4154−4156

methanediolate group formed in situ, which additionally links the trinuclear fragments (Figure 1, inset). Note that formation of the methanediolate group has been found in similar {Fe_6} dimethylbutanate and pivalate clusters.[8]

All Fe atoms in **1** and **2** are in the formal III+ valence state [supported by bond-valence-sum (BVS) values; Table S1 in the SI] and adopt distorted octahedral environments. For **1** and **2**, two "outer" Fe atoms (positions 1 and 4 in Figure 2) are

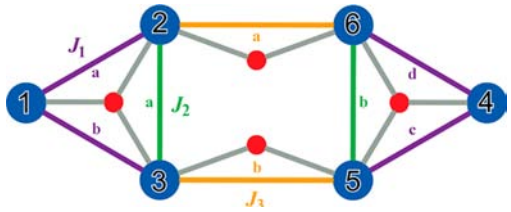

Figure 2. Intracluster coupling scheme of the {Fe_6} cores in **1** and **2**. J_1 contacts correspond to one μ_3-O and two carboxylate bridges, J_2 to one μ_3-O, methanediolate and one carboxylate, and J_3 to one μ_2-O (belonging to methanediolate) and one carboxylate (Fe, blue circles; μ-O, red circles).

coordinated by a μ_3-O atom [Fe−μ_3-O, 1.852(4) and 1.851(4) Å for **1**; 1.869(11) and 1.854(11) Å for **2**], as well as four O atoms from four pivalate groups [Fe−O_{carb}, 2.000(5)−2.025(5) Å (**1**); 1.977(15)−2.021(13) Å (**2**)]. The coordination sphere in **1** is completed by an O atom of diox [Fe−O_{diox}, 2.216(4) and 2.240(5) Å] and in **2** by a N atom of 4,4′-bpy [Fe−N, 2.221(16) and 2.241(14) Å]. For four "inner" Fe atoms, the coordination sphere is completed by four carboxylate O atoms with Fe−O_{carb} distances ranging from 1.990(5) to 2.053(5) Å for **1** and from 1.972(12) to 2.069(13) Å for **2**, a μ_3-O atom with a slightly longer distances of 1.941(4)−1.964(4) Å (**1**) and 1.914(11)−1.953(11) Å (**2**) compared to the terminal Fe atoms, and an O atom from the methanediolate group [1.984(4)−2.003(4) Å in **1** and 1.977(10)−2.01(1) Å in **2**] (Table S4 in the SI). Fe···Fe distances within the trinuclear fragments and between them are very similar to those of the discrete {Fe_6} methanediolate-containing carboxylate clusters[8,9] (Table S3 in the SI). In summary, in **1**, the geometries of the two approximately isosceles Fe_3(μ_3-O) triangles in the {Fe_6} groups match each other relatively closely, whereas in **2**, the Fe_3(μ_3-O) triangles differ more significantly.

Despite the general similarity of the {Fe_6} building blocks in **1** and **2** (Fe···Fe distances differ less than 0.015 Å from their averages; Table S3 in the SI), the observed magnetic low-field susceptibility displays stark differences (Figure 3), which highlight not only the variations in magnetic exchange pathways within the {Fe_6} groups but, more importantly, the significant role of the inter-{Fe_6} coupling mediated either by the diox (closest Fe···Fe contact: 7.17 Å) or 4,4′-bpy (11.39 Å) linkers. Within the {Fe_6} groups of both **1** and **2**, the exchange connectivity in a first approximation is limited to nearest-neighbor interactions that are all mediated by at least one μ-oxo and one μ-carboxylate groups. At first, the magnetism of the {Fe_6} groups is modeled for a minimal number of independent coupling parameters. Assuming two identical isosceles Fe_3(μ_3-O) triangles, three exchange energies (J_{1-3}) are required to describe the coupling interactions between the spin-only (S = $^5/_2$; $^6A_{1g}$) Fe^{III} centers, resulting in the exchange Hamiltonian (cf. Figure 2)

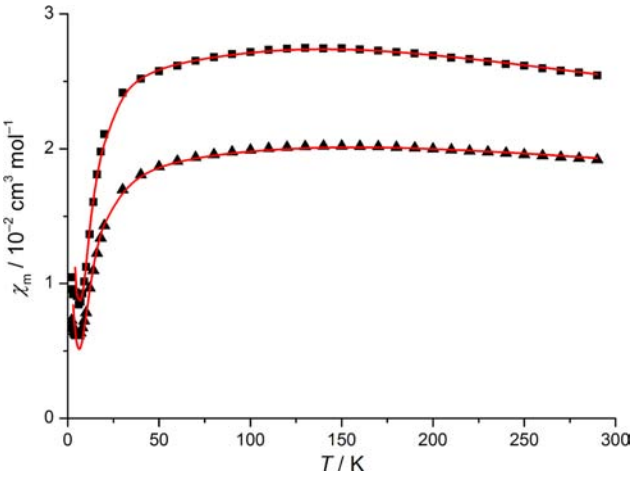

Figure 3. Temperature dependence of the molar susceptibility (χ_m) of **1** (squares) and **2** (triangles) at 0.1 T. Red graphs: least-squares fits to the 8J model Hamiltonian.

$$\hat{H}_{ex} = -2[J_1(\hat{S}_1\cdot\hat{S}_2 + \hat{S}_1\cdot\hat{S}_3 + \hat{S}_4\cdot\hat{S}_5 + \hat{S}_4\cdot\hat{S}_6) + J_2(\hat{S}_2\cdot\hat{S}_3 + \hat{S}_5\cdot\hat{S}_6) + J_3(\hat{S}_2\cdot\hat{S}_6 + \hat{S}_3\cdot\hat{S}_5)] \quad (1)$$

Both **1** and **2** exhibit dominant antiferromagnetic coupling: At 300 K, the $\chi_m T$ values of 7.7 cm^3 mol^{-1} K (**1**) and 5.7 cm^3 mol^{-1} K (**2**) are well below the spin-only limit of 26.25 cm^3 K mol^{-1} (g_{iso} = 2.0). Below broad maxima at ca. 150 K in the molar magnetic susceptibility χ_m versus T curve (Figure 3), the susceptibility steadily decreases, indicating singlet ground states for both **1** and **2**. This observation is supported by the field dependence of the molar magnetization at 2.0 K, with very low magnetization values at 5.0 T (**1**, M_m = 0.08 μ_B; **2**, M_m = 0.06 μ_B). In both cases, the observed slight increase in χ_m below 8 K is caused by a small fraction (ρ) of a paramagnetic S = $^5/_2$ impurity.

The intercluster coupling between neighboring {Fe_6} groups in **1** and **2** (inherently weaker than the intracluster interactions) is described by the phenomenological molecular-field approximation, $\chi_m^{-1} = \chi'^{-1}_m - \lambda_{mf}$, where χ'_m denotes the susceptibility contribution of a discrete {Fe_6} cluster, and a negative value of the molecular-field parameter λ_{mf} corresponds to antiferromagnetic intercluster coupling. Fitting the susceptibility data to the combined 3J−λ_{mf} model with no restraints results in numerous local minima in the quality-of-fit parameter SQ. We thus derive reliable J_{1-3} starting values from empirical structure−property relationships for oxo-bridged iron(III) dimers as a function of the Fe−O distances and bond angles from Werner et al. as well as Weihe and Güdel.[9] Their findings have been parametrized and generalized by applying the AOM, which has been implemented in the computer program *wxJFinder*.[10] Note that the resulting exchange energies (Table S5 in the SI) only reflect the contributions of the oxo (or hydroxo) exchange pathways, but they are considered dominant compared to the methanediolate bridges in **1** and **2**. Fitting is constrained to variations of the three J values that conserve their predicted relative order ($J_1 < J_2 < J_3$). The resulting fits are in good agreement with the experimental data. In addition, as expected, the largest deviation from the starting values is seen for J_3 because here the contribution of the additional carboxylate exchange pathway [vs that of the Fe−O(CH_2)−Fe bridge on the geometry of which the predicted J_3 value is based] becomes more significant. Despite the seemingly

dx.doi.org/10.1021/ic4003884 | *Inorg. Chem.* 2013, 52, 4154−4156

reasonable fits, the wide spread of the J values predicted by *wxJFinder* (Table S5 in the SI), in particular for the less symmetric **2**, indicates that a more detailed exchange coupling model is needed to reflect the physical reality. Yet, accounting for all eight nearest-neighbor exchange energies per $\{Fe_6\}$ cluster would equate even more overparametrization. Thus, a full Hamiltonian was employed in which the individual coupling constants are interrelated:

$$\hat{H}_{ex} = -2\left[J_{1a}\left((\hat{S}_1\cdot\hat{S}_2) + \frac{J_{1b}}{J_{1a}}(\hat{S}_1\cdot\hat{S}_6) + \frac{J_{1c}}{J_{1a}}(\hat{S}_3\cdot\hat{S}_4) + \frac{J_{1d}}{J_{1a}}(\hat{S}_4\cdot\hat{S}_5)\right) + J_{2a}\left((\hat{S}_2\cdot\hat{S}_6) + \frac{J_{2b}}{J_{2a}}(\hat{S}_3\cdot\hat{S}_5)\right) + J_{3a}\left((\hat{S}_2\cdot\hat{S}_3) + \frac{J_{3b}}{J_{3a}}(\hat{S}_5\cdot\hat{S}_6)\right)\right] \quad (2)$$

The J_{nx}/J_{ny} ratios are calculated from the *wxJFinder* results and are kept constant. Thus, no additional independent parameters are introduced, while the fit quality increases significantly (Table 1). We also notice that λ_{mf} changes only minimally between the best fits to the $3J$ (eq 1) and $8J$ (eq 2) models. The difference in λ_{mf} between **1** and **2** primarily reflects the $\{Fe_6\}\cdots\{Fe_6\}$ distance difference; in **2**, the π conjugation in the bpy ligands, and thus their exchange efficiency, is attenuated because of the relatively high torsion angle between the two pyridine groups (26−33°).

Table 1. Magnetochemical Parameters for 1 and 2

	1		2	
J/cm^{-1}	$3J^a$	$8J^b$	$3J$	$8J$
J_{1a} (1···2)	−30.82	−31.21	−32.77	−33.65
J_{1b} (1···3)		−35.89		−28.47
J_{1c} (4···5)		−30.27		−28.27
J_{1d} (4···6)		−34.95		−37.69
J_{2a} (2···3)	−14.43	−16.10	−14.11	−14.76
J_{2b} (5···6)		−14.82		−13.24
J_{3a} (2···6)	−11.75	−12.21	−10.57	−8.39
J_{3b} (3···5)		−12.21		−13.36
$\lambda_{mf}/10^4$ mol m^{-3}	−11.6	−8.91	−0.12	−0.14
ρ/%	0.8	0.8	0.09	0.09
SQ/%^{c}	1.30	0.95	1.29	1.01

^{a}Results for the $3J-\lambda_{mf}$ model (eq 1). ^{b}Results for the $8J-\lambda_{mf}$ model (eq 2) incorporating ratios determined from *wxJFinder* results. ^{c}SQ = $\{(\sum_{i=1}^{n}[(\chi_i^{obs} - \chi_i^{calc})/\chi_i^{obs}]^2)^{1/n}\}^{1/2}$.

In conclusion, hexanuclear iron(III) pivalate $[Fe_6O_2(O_2CH_2)(O_2CCMe_3)_{12}]$ coordination clusters, featuring rare methanediolate groups as central chelating ligands, can be directly interlinked via symmetric N,N′ or O,O′ ligands. The resulting 1D zigzag chain compounds **1** and **2** are characterized by significant antiferromagnetic intercluster exchange interactions. Identifying these unambiguously solely on the basis of temperature-dependent susceptibility data requires reasonable starting values and fitting constraints, which can be determined from the magnetochemically relevant Fe−O substructure of the $\{Fe_6\}$ building groups via *wxJFinder*. Given the chemical versatility of the $\{Fe_6\}$ groups and reliability of the AOM approach to assess their internal coupling, we are currently exploring the formation and magnetochemical interpretation of two- and three-dimensional networks of these spin clusters.

■ ASSOCIATED CONTENT

Supporting Information

Details of the synthesis of **1** and **2**, BVS calculations, details of structural determination, comparison of methanediolate-containing $\{Fe_6\}$ clusters, description of *wxJFinder*, selected bond distances and angles, atom numbering scheme, packing diagrams, and TGA/DTA curves. This material is available free of charge via the Internet at http://pubs.acs.org.

■ AUTHOR INFORMATION

Corresponding Author

*E-mail: paul.koegerler@ac.rwth-aachen.de. Phone: +49-241-80-93642. Fax: +49-241-80-92642.

Funding

Financial support from the EU (POLYMAG, IIF Contract 252984) and from RWTH Aachen University (UROP grants for T.S. and A.M.) is acknowledged.

Notes

The authors declare no competing financial interest.

■ REFERENCES

(1) Jeon, I.-R.; Clerac, R. *Dalton Trans.* **2012**, *41*, 9569−9586. Polunin, R. A.; Kiskin, M. A.; Cador, O.; Kolotilov, S. V. *Inorg. Chim. Acta* **2012**, *380*, 201−210. Zhang, L.; Clerac, R.; Onet, C. I.; Venkatesan, M.; Heijboer, P.; Schmitt, W. *Chem.—Eur. J.* **2012**, *18*, 13984−13988. Roubeau, O.; Clerac, R. *Eur. J. Inorg. Chem.* **2008**, *47*, 4325−4342. Albores, P.; Rentschler, E. *Inorg. Chem.* **2008**, *47*, 7960−7962. Przybylak, S. W.; Tuna, F.; Teat, S. J.; Winpenny, R. E. P. *Chem. Commun.* **2008**, 1983−1985. Turner, D. R.; Pek, S. N.; Cashion, J. D.; Moubaraki, B.; Murray, K. S.; Batten, S. R. *Dalton Trans.* **2008**, 6877−6879.

(2) Baca, S. G.; Malaestean, I. L.; Keene, T. D.; Adams, H.; Ward, M. D.; Hauser, J.; Neels, A.; Decurtins, S. *Inorg. Chem.* **2008**, *47*, 11108−11119.

(3) Malaestean, I. L.; Kravtsov, V. C.; Speldrich, M.; Dulcevscaia, G.; Simonov, Y. A.; Lipkowski, J.; Ellern, A.; Baca, S. G.; Kögerler, P. *Inorg. Chem.* **2010**, *49*, 7764−7772.

(4) Baca, S. G.; Filippova, I. G.; Keene, T. D.; Botezat, O.; Malaestean, I. L.; Stoeckli-Evans, H.; Kravtsov, V. C.; Chumacov, I.; Liu, S.-X.; Decurtins, S. *Eur. J. Inorg. Chem.* **2011**, *3*, 356−367.

(5) Dulcevscaia, G. M.; Filippova, I. G.; Speldrich, M.; van Leusen, J.; Kravtsov, V. C.; Baca, S. G.; Kögerler, P.; Liu, S.-X.; Decurtins, S. *Inorg. Chem.* **2012**, *51*, 5110−5117.

(6) Speldrich, M.; Schilder, H.; Lueken, H.; Kögerler, P. *Isr. J. Chem.* **2011**, *51*, 215−227.

(7) Crystal data for **1**: $C_{65}H_{118}Fe_6O_{30}$, M_r = 1714.7 g mol^{-1}, monoclinic, space group $P2_1/n$, a = 15.192(3) Å, b = 24.745(4) Å, c = 23.761(4) Å, β = 96.654(4)°, V = 8873(3) Å^3, Z = 4, R1 = 0.0488 [$I > 2\sigma(I)$], wR2 = 0.1170 (for 61958 unique reflections and 957 refined parameters). Crystal data for **2**: $C_{81}H_{133}Fe_6N_7O_{28}$, M_r = 2308.9 g mol^{-1}, monoclinic, space group $C2/c$, a = 30.665(7) Å, b = 24.222(5) Å, c = 29.554(9) Å, β = 103.908(5)°, V = 21308(9) Å^3, Z = 8, R1 = 0.1231 [$I > 2\sigma(I)$], wR2 = 0.3486 (for 50908 unique reflections and 964 refined parameters). CCDC 888617 (**1**) and 888618 (**2**).

(8) Murugesu, M.; Abboud, K. A.; Christou, G. *Polyhedron* **2004**, *23*, 2779−2788. Fursova, E. Y.; Romanenko, G. V.; Ovcharenko, V. I. *Russ. Chem. Bull., Int. Ed.* **2005**, *54*, 811−813.

(9) Werner, R.; Ostrovsky, S.; Griesar, K.; Haase, W. *Inorg. Chim. Acta* **2001**, *326*, 78−88. Weihe, H.; Güdel, H. U. *J. Am. Chem. Soc.* **1997**, *119*, 6539−6543.

(10) van Leusen, J.; Kögerler, P. *wxJFinder 1.0*; RWTH Aachen University, 2012, contact wxjfinder@ac.rwth-aachen.de.